

How to quantify tree leaf area index in an open savanna ecosystem: A multi-instrument and multi-model approach

Youngryel Ryu^{a,*}, Oliver Sonnentag^a, Tiit Nilson^b, Rodrigo Vargas^a, Hideki Kobayashi^a, Rebecca Wenk^a, Dennis D. Baldocchi^a

^a Department of Environmental Science, Policy and Management, 137 Mulford Hall #3114, University of California, Berkeley, CA 94720-3114, USA

^b Tartu Observatory, 61602 Tõravere, Estonia

ARTICLE INFO

Article history:

Received 1 June 2009

Received in revised form 17 August 2009

Accepted 18 August 2009

Keywords:

Leaf area index

Clumping index

Gap fraction

Leaf inclination angle

Savanna

Heterogeneity

ABSTRACT

Savannas are spatially heterogeneous, open ecosystems, thus efforts to quantify canopy structure with methods developed for homogeneous, closed canopies are prone to failure. We examine the applicability of two direct (litterfall, allometry) and five indirect (LAI-2000, TRAC, digital hemispheric photography, digital cover photography, traversing radiometer system) methods to determine leaf area index across a 9 ha domain in an oak-savanna ecosystem in California, USA. Interpretation of the leaf area index measurements is supported by two gap-fraction models. We recommend that leaf inclination angle distribution should be characterized first. For this purpose, we propose a simple, reliable and reproducible method using a digital camera. We show that the combination of digital cover photography and LAI-2000 could provide spatially representative leaf area index, gap fraction and element clumping index. Based on these two indirect methods, we quantify spatially representative element clumping index and leaf area index at ecosystem scale as 0.49 ± 0.10 (mean \pm 95% confidence interval) and 0.77 ± 0.27 , respectively. In contrast to previous studies in northern ecosystems, measurement and modeling results suggest that element clumping index decreases with view zenith angle, most likely due to apparent changes of tree distribution pattern with the view zenith angle. Our results highlight the importance of ecosystem-scale clumping effects for the adequate quantification of tree leaf area index in savannas. Finally, we suggest a protocol to quantify leaf area index and its associated canopy structure variables in open canopy ecosystems.

© 2009 Elsevier B.V. All rights reserved.

1. Introduction

Savannas exist in water-limited regions where potential evaporation exceeds precipitation (Baldocchi and Xu, 2007; Joffre et al., 2007; Ryu et al., 2008). As a result, savannas have evolved with heterogeneous, open canopies (Eagleson and Segarra, 1985; Rodriguez-Iturbe et al., 1999; Sankaran et al., 2004). This canopy openness presents a challenge for evaluating tree leaf area index (L , nomenclature is summarized in Appendix A), as most methods were developed for ideal and closed canopies (e.g. Welles and Norman, 1991). To date, only a few studies have used indirect methods in savannas (Hoffmann et al., 2005; Privette et al., 2004; Scholes et al., 2004), yet critical questions remain unanswered: What are the strengths and weaknesses among the methods? How can we reliably measure L indirectly in a savanna?

The questions asked in the study are critical because L , one-sided leaf area per unit ground area (Watson, 1937), is a key

variable to link structure and function of ecosystems. First, the intercepted radiation is mainly determined by L , and is related directly to the amount of CO₂ assimilation through photosynthesis (dePury and Farquhar, 1997; Norman, 1982). Second, L has implications for hydrological ecosystem dynamics because L controls rainfall interception (Aston, 1979), canopy evapotranspiration (Baldocchi et al., 2002; Leuning et al., 1995), and soil evaporation (Kelliher et al., 1995; Schulze et al., 1994). Third, L determines the area involved in emissions and depositions of trace gases such as isoprene, NO_x and SO_x (Baldocchi et al., 1999; Hicks et al., 1987).

Direct and indirect methods are used to quantify L , but there are several challenges and limitations for their application in savannas. Direct methods include the collection of leaves through either destructive sampling (Gower and Norman, 1991), litterfall traps (Marshall and Waring, 1986), allometric relations (Gower and Norman, 1991), or using the stratified-clip method (Hutchinson et al., 1986; Monsi and Saeki, 1953). Indirect methods use mathematical and radiative transfer theory to estimate L from more easily and faster measurable variables such as contact number (K) and gap fraction (P_o). For the inclined point quadrat

* Corresponding author. Tel.: +1 510 642 9048; fax: +1 510 643 5098.
E-mail address: yryu@berkeley.edu (Y. Ryu).

method, a thin probe inserted at a certain angle into short canopies counts the number of contacts between probe and leaves to calculate L (Warren Wilson, 1959, 1960). The measurement of P_o allows estimation of L regardless of canopy height. Most commercially available instruments for the indirect optical measurement of L such as the LAI-2000 plant canopy analyzer (LI-COR, Lincoln, NE, USA) or hemispherical photography (Bonhomme and Chartier, 1972; Neumann and Den Hartog, 1989; Zhang et al., 2005) are based on the P_o theory (e.g. Nilson, 1971). It should be noted that P_o theory-based indirect methods assume closed and homogeneous canopies.

To obtain spatially representative P_o estimates using indirect methods, we have to address questions related to sampling design, instrument performance, and P_o averaging method at the ecosystem scale. Sampling design for P_o measurements is crucial in heterogeneous, open canopies but has not been fully explored. Because of savannas' canopy openness and heterogeneity and instrument accuracy, determination of the adequate method to measure P_o is elusive but critical. Thus, it is essential to evaluate and constrain indirect measurements of P_o with independent P_o models. Another important issue is the averaging of P_o (i.e. $\ln(\overline{P_o})$ vs $\overline{\ln(P_o)}$) (Fassnacht et al., 1994; Lang and Xiang, 1986), which may result in different estimates of L . We could expect that two P_o averaging methods may result in similar L estimates for homogeneous, closed canopies. In contrast, increasing spatial variability of P_o may result in substantially different L estimates. We postulate that in heterogeneous savanna ecosystems the difference between the two P_o average methods would be very different as reported by Lang and Xiang (1986).

Another critical variable used for indirect methods in heterogeneous savannas is the clumping index (Ω). This index quantifies the spatial distribution pattern of leaves (Nilson, 1971; Norman and Jarvis, 1974). It has been usually quantified based on gap size distribution measured from Tracing Radiation and Architecture of Canopies instrument (TRAC; 3rd Wave Engineering, ON, Canada) or digital hemispherical photography (DHP) (Chen and Cihlar, 1995; Leblanc, 2002; Leblanc et al., 2005; Norman and Jarvis, 1974; van Gardingen et al., 1999). Main challenges to quantify and interpret Ω in savannas include the range of view zenith angle (θ_v), the type of calculation methods, and how Ω changes with θ . Because Ω changes with θ (Andrieu and Sinoquet, 1993; Chen, 1996; Kucharik et al., 1999; Norman and Welles, 1983), several Ω values covering a wide range of θ are required to calculate hemispherical average Ω value. The length and number of transects and sampling time must be compromised to obtain spatially representative $\Omega(\theta)$ that covers zero to $\pi/2$ of θ adequately because the TRAC instrument has to be walked at slow pace ($\sim 0.3 \text{ m s}^{-1}$) (Leblanc et al., 2002). Most studies using the TRAC instrument are based on a limited number of $\Omega(\theta)$ estimates within narrow and moderate range of θ including 30–80° (Chen, 1996), 25–50° (Law et al., 2001), 30–50° (Hall et al., 2003) and 57.5° (Jonckheere et al., 2005). However, few studies have examined whether those narrow range estimates of $\Omega(\theta)$ are sufficient to be spatially representative. Various approaches have been proposed to calculate Ω , namely Lang and Xiang (1986) (hereinafter LX), Chen and Cihlar (1995) (hereinafter CC), and the combination of LX and CC (Leblanc et al., 2005) (hereinafter CLX). Importantly, there was considerable difference among different methods to calculate Ω . For example, based on 29 boreal forest site measurements, Leblanc et al. (2005) reported the mean Ω values calculated from CC, LX and CLX are 0.9, 0.79 and 0.67, respectively. Finally, angular dependence of Ω is an important characteristic to determine spatially representative Ω value. Previous studies from boreal and temperate forests reported that Ω increased with θ (Chen, 1996; Kucharik et al., 1999; Leblanc et al., 2005), yet it is unclear whether this relation is valid in savanna canopies.

Another key variable for the indirect quantification of L is the leaf inclination angle (θ_L), commonly defined as the angle between the leaf surface normal and the zenith (Ross, 1981). The leaf inclination angle distribution function $f(\theta_L)$ describes the leaf inclination angle distribution as the probability density function (de Wit, 1965; Idso and de Wit, 1970). The $f(\theta_L)$ plays a fundamental role in the leaf projection function (commonly referred to as G -function), which describes the projection of unit foliage area on the plane perpendicular to the view direction (Myneni et al., 1989; Ross, 1981). The G -function is essential to calculate P_o at specific view zenith angles. In spite of its importance, most studies assume spherical $f(\theta_L)$ because of the difficulty in estimating θ_L . Various instruments for the in situ measurement of θ_L have been proposed (Kucharik et al., 1998a; Lang, 1973; Smith and Berry, 1979; Smith et al., 1977), but their wide-spread use has been generally hampered due to difficulties in applying them to tall canopies, and due to their unsatisfactory ability to reproduce measurements. Several sophisticated approaches including a 3-dimensional digitizer (Falster and Westoby, 2003; Sinoquet et al., 2009) and a ground based light detection and ranging (LiDAR) (Hosoi and Omasa, 2007) have quantified 3-dimensional leaf arrangement but high economic costs prevent their routine application. Thus, development of a robust, affordable method that allows for reproducible measurements of θ_L regardless of canopy height is warranted. Here we introduce a digital photography based method that meets these criteria.

The goal of this study is to determine spatially representative tree L at ecosystem scale in an oak-savanna canopy in California, USA. To achieve this goal, we measured θ_L , characterized P_o and Ω based on multiple indirect methods and models, and finally quantified L , which we evaluated with directly measured L . The scientific questions we address include: (1) What are the strengths and weaknesses of multiple methods to assess L in heterogeneous, open canopies? (2) How to estimate spatially representative Ω in a savanna? We hypothesize that: (1) Ω may increase with θ in a heterogeneous savanna as reported in previous studies (Chen, 1996; Kucharik et al., 1999). This is expected because longer path lengths with increasing θ would decompose large gaps into smaller ones (i.e. less clumped); and (2) the influence of gaps between crowns on total P_o may be dominant in the savanna site because of the open canopy. Finally, we suggest a protocol to quantify L and its associated canopy structure variables in open canopy ecosystems.

2. Theoretical background

2.1. Leaf projection function and leaf inclination distribution function

The leaf projection function (G) is the projection coefficient of unit foliage area on a plane perpendicular to the view direction (Ross, 1981). The quantification of G requires knowledge of $f(\theta_L)$. Several approaches have been developed to characterize $f(\theta_L)$ including a non-parametric function (de Wit, 1965), an one-parameter ellipsoidal distribution function (Campbell, 1990), and a two-parameter Beta-distribution function (Goel and Strebel, 1984). The two-parameter Beta-distribution function has recently been identified as being the most accurate for describing the probability density of θ_L (Wang et al., 2007):

$$f(t) = \frac{1}{B(\mu, \nu)} (1-t)^{\mu-1} t^{\nu-1} \quad (1)$$

where μ and ν are two parameters, t is $2\theta_L/\pi$, θ_L is leaf inclination angle, and $B(\mu, \nu)$ is the Beta-distribution (Pitman, 2006):

$$B(\mu, \nu) = \int_0^1 (1-x)^{\mu-1} x^{\nu-1} dx = \frac{\Gamma(\mu)\Gamma(\nu)}{\Gamma(\mu+\nu)} \quad (2)$$

where Γ is Gamma function. Assuming a uniform distribution of leaf azimuth orientation, G may be expressed as (Warren Wilson, 1960, 1967):

$$G(\theta) = \int_0^{\pi/2} \phi(\theta, \theta_L) f(\theta_L) d\theta_L \quad (3)$$

$$\phi(\theta, \theta_L) = \begin{cases} \cos \theta \cos \theta_L & |\cot \theta \cot \theta_L| > 1, \\ \cos \theta \cos \theta_L [1 + \left(\frac{2}{\pi}\right)(\tan \vartheta - \vartheta)], & \text{otherwise} \end{cases} \quad (4)$$

where θ is solar zenith angle and $\vartheta = \cos^{-1}(\cot \theta \cot \theta_L)$. Values for $G(\theta)$ range from zero to one and generally converge at ~ 0.5 for all $f(\theta_L)$ when θ is 1 radian ($\approx 57^\circ$) (Lang et al., 1985; Nilson, 1971; Ross, 1981; Warren Wilson, 1960).

2.2. Gap fraction and leaf area index

Monsi and Saeki (1953, 2005) first proposed P_o theory. Under certain conditions the probability of beam penetration can be described by the Poisson distribution:

$$P_o(\theta) = \exp\left(\frac{-G(\theta)L_t}{\cos \theta}\right) \quad (5)$$

where $P_o(\theta)$ is the gap fraction in dependence of solar zenith angle (θ) and L_t is total plant area index that includes leafy and woody components. The main assumption underlying Eq. (5) is that the positions of phytoelements are randomly distributed. By taking the logarithm of Eq. (5), the contact number (K) can be derived:

$$K(\theta) = -[\ln P_o(\theta)] \cos \theta = G(\theta)L_t \quad (6)$$

The inverse estimation of L_t from P_o measurements (Eq. (6)) requires knowledge of G , which is usually unknown. To overcome this limitation, Miller (1967) proposed a theorem for the inverse estimation of L_t that does not require a prior knowledge of the $G(\theta)$:

$$L_t = 2 \int_0^{\pi/2} K(\theta) \sin \theta d\theta = 2 \int_0^{\pi/2} -[\ln P_o(\theta)] \cos \theta \sin \theta d\theta \quad (7)$$

Eq. (7) forms the underlying principle of the LAI-2000 instrument by using diffuse radiation to avoid the strong dependency of the direct solar beam to latitude and seasonality (Welles and Norman, 1991). Another approach to avoid *a-priori* knowledge of the $G(\theta)$ is to measure $P_o(\theta)$ at $\theta = 1$ radian. If the direct beam radiation is used to estimate L_t other than 1 radian θ , then one must quantify $G(\theta)$ as shown in Eq. (3).

To consider the non-random spatial distribution of leaves, Nilson (1971) first proposed a Markov-chain model introducing an additional quantity, Ω , into Eq. (5):

$$P(\theta) = \exp\left(\frac{-G(\theta)L_t\Omega(\theta)}{\cos \theta}\right) \quad (8)$$

Clumping index is expressed as follows: (Chen, 1996):

$$\Omega = \frac{\Omega_E}{\gamma_E} \quad (9)$$

where Ω_E is element clumping index that quantifies foliage clumping at scales larger than the shoot and γ_E is the needle-to-shoot area ratio for shoot-scale clumping. Usually, γ_E is assumed to be 1 for deciduous broad-leaved trees (Chen, 1996).

Retrieval of L_t on the basis of measured P_o θ and inversion of Eq. (7) results in effective leaf area index (L_e) which includes the contribution of all light-intercepting canopy elements (including green and dead leaves, branches, trunks and attached mosses and lichen) assuming their random distribution in space (Black

et al., 1991):

$$L_e = L_t \times \Omega \quad (10)$$

For a random spatial distribution of all light-intercepting canopy elements (i.e. $\Omega = 1$) $L_e = L_t$. A limitation of P_o based approaches is their inability to discriminate between canopies' woody components including attached mosses, lichens, dead leaves, branch and stems from green foliage. For ecosystem with moderate to high values for L , leaves cover most woody components and the probability of a direct beam radiation to hit the woody component is very low (Kucharik et al., 1998b). Thus, the effect of woody components on the P_o estimate may be marginal and ignorable. However, in ecosystems with lower values for L such as savannas, the contribution of woody components to P_o estimate may not be ignorable, and we decided to subtract woody area index (W) (Privette et al., 2004) from L_t in Eq. (10):

$$L = \frac{L_e}{\Omega} - W \quad (11)$$

Obtaining spatially representative estimates of L_e , Ω , W and L is challenging in a heterogeneous ecosystem. In this study, we show the acquisition of each variable based on multiple instruments and models.

3. Methods

3.1. Site description

The study site is Tonzi Ranch (latitude: 38.431°N; longitude: 120.966°W; altitude: 177 m) located in the lower foothills of the Sierra Nevada Mountains, Ione, CA, USA. The site is part of AmeriFlux (<http://public.ornl.gov/ameriflux/>) and is classified as an oak-grass savanna woodland. The site is on flat terrain (average slope: 1.5°) and experiences Mediterranean-type climate with dry, hot summers and rainy, mild winters. Annual average temperature and annual precipitation are 16.9 °C and 565 mm, respectively (1949–2005 climate normals from Camp Pardee climate station; latitude; 38.25°N; longitude: 120.85°W). The overstory consists of dominant blue oak trees (*Quercus douglasii*) with occasional (<10%) grey pine trees (*Pinus sabiniana*). The understory is mainly composed of grasses and forbs (*Brachypodium distachyon*, *Hypochaeris glabra*, *Bromus madritensis*, *Cynosurus echinatus*) (Baldocchi et al., 2004). Due to the low density of grey pine trees (*Pinus sabiniana*), we assumed $\gamma_E = 1$ and thus $\Omega = \Omega_E$ (Eq. (9)). The stem density was 144 ha⁻¹, tree height was 9.4 ± 4.3 m (mean ± standard deviation), trunk height was 1.8 ± 1.3 m, diameter at breast height (DBH) was 0.26 ± 0.11 m, mean crown radius was 2.9 ± 1.4 m, and canopy cover was 0.47 (Chen et al., 2008). More detailed site information may be found in previous studies (Baldocchi et al., 2004; Chen et al., 2008; Ma et al., 2007).

3.2. Sampling design, measurements, and data processing

3.2.1. Sampling design

We established a 300 m × 300 m sampling plot with the micrometeorological tower at the center and gridded at 30 m × 30 m intervals (Fig. 1a). The extent of the plot corresponds to the scale of spatial heterogeneity as determined through semivariogram analysis (Kim et al., 2006). A grid size of 30-m was chosen to minimize oversampling by different instruments. For example, the field-of-view of the LAI-2000 instrument is approximately three times the canopy height (~ 27 m). Field data was collected with the LAI-2000, TRAC, DHP, and digital cover photography (DCP) from Aug 5 to Aug 7, 2008, i.e. near the peak of the growing season (Table 1). Technical problems with an automatic traversing radiometer system (TRS) required us to use

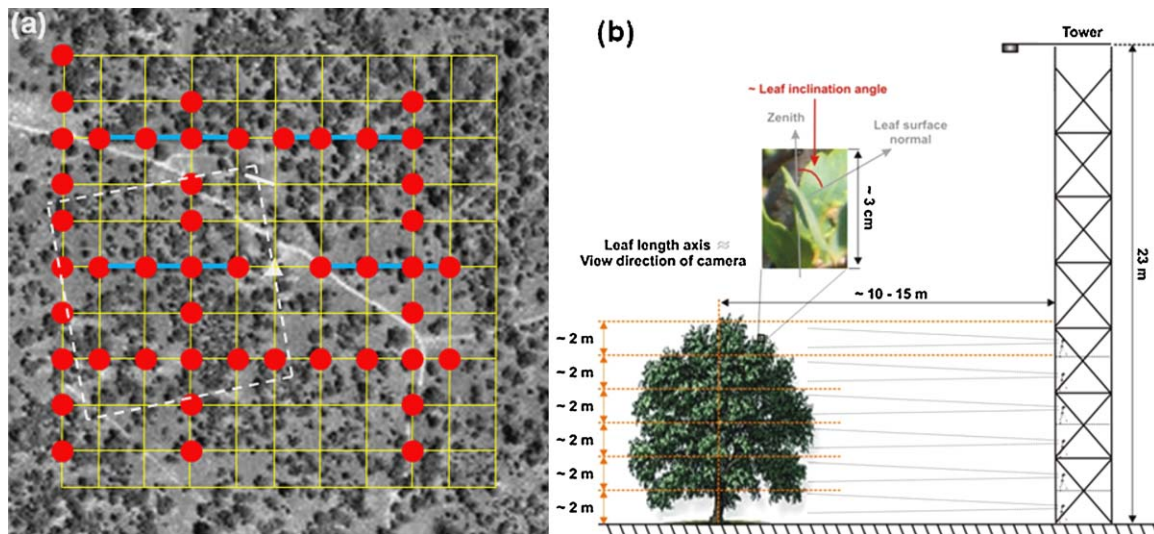


Fig. 1. (a) Plot design laid over IKONOS image taken on Sep 2001. The eddy covariance flux tower is located at the center (white triangle). The plot extent was 300 m × 300 m, which was subdivided with a 30 m × 30 m grid. LAI-2000 was measured at all intersected points of gridded yellow line of the subplots (i.e. 121 points). DHP and DCP were measured at red circles. TRAC was measured over four sub-transects (blue lines). Litterfall collectors were installed in a 25 m × 25 m grid within a 150 m × 150 m plot (dashed white line) within the foot print of the tower and the large 300 m × 300 m plot. Traversing radiometer system was located north of the flux tower (white line). (b) A schematic diagram of protocol used to measure leaf inclination angle (not drawn to scale). (For interpretation of the references to colour in this figure legend, the reader is referred to the web version of the article.)

data from three days (25, 27, and 29 July 2008) close to the intensive field measurement dates. To estimate woody area index (W), we made 33 additional measurements of LAI-2000 along three transects during the leafless period on 31 Jan 2009, and 58 additional measurements of DCP at the same three transects ($n = 33$) and at the litterfall trap locations ($n = 25$) (see Section 3.2.8) on Mar 16, 2009. In 2006, we installed a 150 m × 150 m subplot directly upwind of the flux sensor (Fig. 1a) to develop an independent estimate of the woodland carbon budget from direct measures of primary production. As part of this effort, we inventoried all the trees and installed 25 litterfall traps (opening area = 0.16 m²; height = 1.5 m) at regular intervals (25 m apart) in the interior of the plot. Table 1 summarizes the description of instruments. In the following sections, we first explain the leaf inclination angle measurement, then indirect instruments to estimate L , and lastly direct methods to estimate L employed in this study.

3.2.2. Leaf inclination angle

We used a high definition digital camera (LUMIX, Panasonic DMC-F250, Secaucus, NJ, USA) using a fixed zoom lens (10×) and leveled by a 1.3 m tripod to measure θ_L . We took digital

photographs of the surrounding oak canopy (north, east, west, south) using the tower (Fig. 1b). Photographs in all four directions were taken at six height levels at 2 m increments. An average of around 50 images per level resulted in a total of 304 images. Total 11 trees contributed θ_L measurements. Because of the big holes within crowns, we also took the inner crown leaves. To comply with the definition of θ_L , we only selected leaves oriented approximately parallel to the viewing direction of the camera (Fig. 1b). We only selected leaves seen as line to exclude bent leaves. We manually estimated θ_L using the angle measurement tool of a public domain image processing software (ImageJ; <http://rsbweb.nih.gov/ij/>). At each height level, we measured θ_L for 200 leaves resulting in a total of 1200 leaves for all levels.

3.2.3. LAI-2000

The LAI-2000 instrument measures $P_o(\theta)$ at five concentric rings (ring 1: 0–13°; ring 2: 16–28°; ring 3: 32–43°; ring 4: 47–58°; ring 5: 61–74°) over the hemisphere based on the detection of blue diffuse light (400–490 nm) penetrating the canopy (Welles and Norman, 1991). One LAI-2000 unit continuously recorded (15 s interval) blue diffuse light at the top of the tower as reference. Using a second LAI-2000 unit, an operator took one measurement

Table 1
Description of measurements, processing, and characteristics of indirect instruments to estimate L employed in this study.

	LAI-2000	Tracing radiation and canopy architecture (TRAC)	Digital hemispheric photography (DHP)	Digital cover photography (DCP)	Traversing radiometer system (TRS)
Spatial sampling number (sampling number in leafless dates)	121 (30)	4	47	47 (58)	1
Transect length. (raw data acquisition frequency)	–	90-m (32 Hz)	–	–	30-m (10 Hz)
Number of view zenith angles	5 (no exclusion of outer rings)	1	various	1 (zenith)	1
Range of view zenith angles ^a	7–68	25–77	10–80	0–13	19–80
Calculation method of clumping index in this study	–	CC ^b , CLX ^c	CC, CLX	CC	CC, CLX
Necessity of leaf inclination angle information to get L_e^d	X	O	X	O	O
Illumination condition	Diffuse	Direct	Diffuse	Direct/diffuse	Direct

^a Ranges about TRAC, DCP and RTC were obtained from several measurements at different solar zenith angles.

^b Chen and Cihlar, 1995.

^c Combination of LX and CLX (Leblanc et al., 2005).

^d Effective leaf area index.

at each measurement location when sun is lower than the top of canopy to make sure diffuse sky condition. A 180° view cap was used on each sensor to avoid the appearance of the operator on the sensor and block potentially remaining direct light. The operator always stood between the sensor and the declining sun. Throughout this paper, we used L_e derived from $\ln(\overline{P_o}(\theta))$ approach to avoid over-correction of clumping effect (Ryu et al., to be submitted for publication).

3.2.4. Tracing radiation of canopy and architecture

The TRAC instrument allows for the indirect measurement of Ω_E , L_e and L_t in the field based on a gap size distribution theory (Chen and Cihlar, 1995; Leblanc et al., 2005). We used the TRAC instrument along four 90 m EW-oriented segments (Fig. 1a). To estimate spatially representative Ω_E , we employed TRAC instrument at each transect segment in approximately two-hour intervals over the course of a day and thus at different values for θ , resulting in five raw data sets per transect segment. All TRAC measurements were post-processed using the TRACWin software (v4.1.1) (Leblanc, 2008).

From each transect measurement, the accumulated P_o derived from the measured gap-size distribution function determines $P_o(\theta)$ (Chen and Cihlar, 1995; Leblanc, 2002). We averaged $P_o(\theta)$ measured from four transects over 10-degree intervals of θ and we used the $\overline{P_o}(\theta)$ in Eq. (7) to calculate L_e . We calculated two sets of $\Omega_E(\theta)$ using CC and CLX methods as provided by TRACWin software, and then calculated Ω_E for each method as:

$$\Omega_E = \frac{\int_m^M \Omega_E(\theta) \sin(\theta) d\theta}{\int_m^M \sin(\theta) d\theta} \quad (12)$$

where M and m are maximum and minimum θ , respectively.

3.2.5. Digital hemispherical photography

With digital hemispherical photography, estimates of Ω_E , L_e and L_t are obtained by measuring P_o and gap-size distribution (Leblanc, 2008). We randomly selected three north-south transects and three east-west transects with a total length 270 m (Fig. 1a). At each measurement point, we took a hemispherical photograph. All DHPs were taken with a 4 mega pixels Nikon CoolPix4500 digital camera using the finest available resolution, and a FC-E8, Nikon fisheye lens with a field-of-view of 183° was attached to the camera. All photographs were taken near sunset or sunrise. We chose the following settings for the camera: (1) manual mode, (2) fish-eye lens, fixed with centrally weighted exposure for automatic exposure; (3) manual mode aperture for fixed exposure; (4) high image quality (2272 × 1704 pixel matrix) and (5) JPEG format. Photographs were taken from the sky reference exposure and then corrected with two stops more exposure relative to the open sky conditions (Zhang et al., 2005). At the end of each transect, the open sky conditions were recalibrated because we were able to access open areas easily. The reference sky exposure was always determined with the same camera in an opening with no obstruction above 15° of the solar zenith angle in all directions using an aperture of F5.3 (Zhang et al., 2005). Digital image processing of the hemispherical images was done using the DHP software v4.5.2 (Leblanc, 2008; Leblanc et al., 2005). Thresholds to distinguish leaf from sky were selected manually following the protocol of Zhang et al. (2005), and all photographs were processed by the same person. We used a gamma, the factor to enhance raw image of 2.2 (Leblanc, 2008). We averaged $P_o(\theta)$ measured from 47 pictures over every 5 degree interval of θ_v and we used $\overline{P_o}(\theta)$ as an input to Eq. (7) to calculate L_e . We averaged Ω_E from 47 pictures using CC and CLX methods provided by TRACWin software in DHP mode.

3.2.6. Digital cover photography

With digital cover photography, estimates of foliage and crown cover fractions, and crown porosity based on zenith view direction digital photographs taken from below the canopy are obtained. Finally, estimates of $\Omega_E(0)$ and L_t can be derived (Macfarlane et al., 2007a,b). The camera (Nikon CoolPix4500, 2272 × 1704 resolution) was set to automatic exposure, aperture-priority mode, minimum aperture and F2 lens (Macfarlane et al., 2007b). The camera was leveled and the lens was pointed towards zenith. This setup provides a view zenith angle (θ_v) from 0 to 15°, which is comparable with the 1st ring in LAI-2000 (Macfarlane et al., 2007b). Before sunset or after sunrise when sun is lower than the top of canopy, a total of 47 photos were taken at the same measurements locations together with DHP from Aug 5 to Aug 7, 2008. The key input parameter to estimate L_t is the $G(0)$, and we used 0.44 estimated from measured θ_L (see Section 4.1). To estimate W from photos taken at a leafless date, the inclination angle of woody components is necessary, which were not systematically quantified in this study. Instead, we took photos at horizontal view for each DCP measurement points thus combination of zenith view and horizontal view photos gave some sense on the branch architecture at each point. Based on the photos and two limits of G at zenith direction (i.e. 0.85 for planophile and 0.45 for erectophile in Fig. 2b), we visually determined $G(0)$ of dominant woody components at each DCP

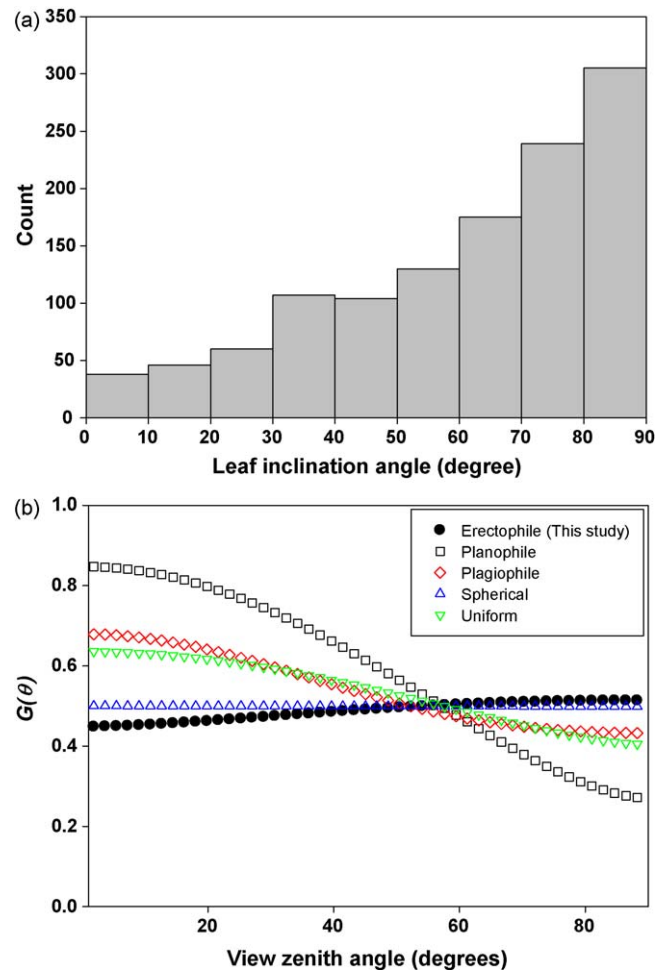


Fig. 2. (a) Histogram of leaf inclination angle. This includes all samples measured from six canopy levels that span from 1 to 11 m. (b) Leaf projection function (G) against view zenith angle (θ_v). Erectophile was drawn based on the developed leaf inclination angle distribution function in this study. Planophile, plagiophile, spherical, and uniform cases were drawn for comparison based on de Wit (1965).

measurement point. We averaged foliage cover fraction and canopy cover fraction from all pictures including non-canopy photos, and then estimated spatially representative $\Omega_E(0)$ that explicitly considers large gaps. The cover images were analyzed using Adobe Photoshop CS4 (Adobe Systems Incorporated, San Jose, CA, USA) following Macfarlane et al. (2007b).

3.2.7. Traversing radiometer system

A traversing radiometer system measured incoming and outgoing photosynthetically active radiation (PAR), and net radiation under canopies. A 30-m rail track was setup 1-m above the ground at 60 m apart from the tower (Fig. 1a). About half of the rail track was situated below the canopy while other half was situated in open space. Two PAR sensors (incoming and outgoing PAR measurements, PAR LITE, Kipp & Zonen, The Netherlands) and one net radiation sensor (NR-LITE-L, Kipp & Zonen, The Netherlands) moved along the rail track at 0.04 m s^{-1} . One round trip took about 24 min. All radiation measurements were made at a frequency of 1 Hz. The data was transferred to a common personal computer set-up at the tower via a wireless local area network. The up- and down-facing PAR sensors continuously recorded incoming and outgoing PAR over the daytime at the same transect, so it may be treated as TRAC-like data. We used the incoming PAR data as input to TRACWin software, and then we estimated $P_o(\theta)$, Ω_E and L_e with same procedures of TRAC data processing (Section 3.2.4).

3.2.8. Allometry

Diameter at breast height (1.37 m) of all the trees in the subplot (Fig. 1a) was measured in 2006. Subsequently, annual growth was monitored on a random subset of 140 trees with dendrometer bands. We used these annual growth estimates to project 2008 diameters for all live trees in the carbon subplot. We then used allometric relationships for blue oak (Karlik and McKay, 2002) to predict leaf area as a function of tree diameter. The allometry based L was calculated as the sum of the leaf area per tree divided by the total plot area ($22,250 \text{ m}^2$).

3.2.9. Litterfall

In 2008, litter was collected three times from the traps in the subplot (Fig. 1a) with the last collection timed soon after last leaf fall. Litter was separated into leaves, twigs, and seeds and then oven-dried to a constant weight. We used the sum of these sequential collections to get a total leaf biomass per collector. Specific leaf area (SLA) was determined for a subset ($n = 48$) of oak leaves obtained from the tree times collection. We measured the one-sided area of 10 fresh oak leaves per sample (total leaf number is 480) with the LI-3100C Area Meter (LI-COR, Lincoln, NE, USA). These samples were then dried to a constant weight. Based on these measurements, the mean SLA for blue oak leaves was $91.8 \text{ cm}^2/\text{g}$ (standard error = $1.18 \text{ cm}^2/\text{g}$). LAI per trap was calculated as leaf biomass per trap \times SLA and then the mean of these 25 values was taken as the best measure as litterfall L for the subplot. There were two individuals of the evergreen tree, grey pine, present within our plot. However no pine needles were found in the traps in 2008. Given the rarity of the pines (2 trees) compared to the oaks (316 trees), we ignored them in our estimates of both allometry based L and litterfall L .

3.3. Gap-fraction models

To test P_o and Ω_E estimates from the indirect instruments, we used a gap-fraction model that explicitly considers clustering of foliages into crowns (Nilson, 1999; Nilson and Kuusk, 2004), and a 3-dimensional radiative transfer model (Kobayashi and Iwabuchi,

2008). Nilson (1999) determines P_o as follows:

$$P_o(\theta) = \exp[-c(\theta)NS(\theta)] \quad (13)$$

where

$$c(\theta) = \frac{-\ln[1 - (1 - P_1(\theta))(1 - GI)]}{1 - GI} \quad (14)$$

and

$$P_1(\theta) = \exp\left[\frac{-G(\theta)(L/\gamma_E + B)}{(NS(\theta) \cos \theta)}\right] \quad (15)$$

where N is the tree density (trees m^{-2}), $S(\theta)$ is the area of projection of the average tree crown envelope on the horizontal plane, $P_1(\theta)$ is the mean P_o in a single tree crown at θ , B is the branch area index, and GI is the relative variance of the number of trees in the area $S(\theta)$ (Fisher's dispersion index, Appendix B) (Fisher, 1954). By assuming that Eq. (8) and (13) give same $P_o(\theta)$, $\Omega_E(\theta)$ may be expressed as follows:

$$\Omega_E(\theta) = \frac{c(\theta)NS(\theta) \cos \theta}{(G(\theta)(L/\gamma_E + B))} \quad (16)$$

By using $P_o(\theta)$ measured from LAI-2000 during the leafless period as input data into Eq. (13), B may be quantified (Nilson and Kuusk, 2004). Thus, the combination of $P_o(\theta)$ measured from LAI-2000 on a leafless date with Nilson (1999) model allows to estimate W as follows:

$$W = B + T \quad (17)$$

$$T = \pi \times R \times h \times N \quad (18)$$

where T is trunk area index, R is the mean trunk radius (m), and h is the trunk height (m). Additionally, the model distinguishes gaps between crowns and within crowns. The required canopy structure input parameters were obtained from an airborne LiDAR measurement that was taken across a $200 \text{ m} \times 200 \text{ m}$ domain including the tower at the center in 2003 (Chen et al., 2007a,b). The LiDAR used discrete return and the average posting density was 9.5 points per square meter. Another key input variable is $f(\theta_L)$ measured using a digital camera (see Section 3.2.2).

The model of Kobayashi and Iwabuchi (2008) explicitly considers individual tree shapes and positions derived from LiDAR measurement. Similar to Nilson (1999), $f(\theta_L)$ is a key input parameter. Because of pre-determined tree positions and shapes, $P_o(\theta)$ at specific locations can be calculated without Ω_E (i.e. Eq. (5)). Within the area covered by the LiDAR scene, we selected a total of 100 points every 20 m. At each point, we calculated $P_o(\theta)$ from 5 to 80 degrees of θ with a 5 degree interval, and then we determined spatially representative $P_o(\theta)$ by averaging all points' $P_o(\theta)$ values. By inverting Eq. (8) with input of $P_o(\theta)$, spatially representative $\Omega_E(\theta)$ may be quantified. Both models require L_t as an input parameter. We used 1.14 of L_t as a sum of 0.82 of litterfall L and 0.32 of W that was derived from DCP measurements (see Section 4.4.).

3.4. Uncertainty and statistical analyses

To investigate the uncertainty associated with sampling design, we used the gridded LAI-2000 measurements within the $300 \text{ m} \times 300 \text{ m}$ area (Fig. 1a). To study the impact of sample size, we selected sample sizes from 1 to 121. For each sample size, we created 10,000 data sets by drawing random subsets of the respective size from all 121 measurements without replacement. Next, we separately calculated the coefficient of variation (standard deviation/average, CV) for the gap fraction of each ring of the LAI-2000 instrument. To study the impact of plot extent, we

Table 2
Leaf inclination angle measured at six height levels (mean ± 95% confidence interval).

	2-m	4-m	6-m	8-m	10-m	12-m	Total
Leaf inclination angle	57 ± 3.3	58 ± 3.1	62 ± 3.1	61 ± 3.1	66 ± 2.9	65 ± 3.0	62 ± 1.3

used plot sizes from 30 to 270 m over 30 m intervals. For each plot size, we randomly resampled 10,000 plots without replacement within 300 m × 300 m area, and then generated the CV for L_e .

To quantify error propagation in the calculation of L_e , Ω_E , W , and L , we used the method of moments (Taylor, 1997):

$$s_{\bar{y}} = \sqrt{\sum_{j=1}^n \left(\frac{\partial y}{\partial x_j} s_{\bar{x}_j}\right)^2 + 2 \sum_{j=1}^{n-1} \sum_{k=j+1}^n r_{x_j x_k} \left(\frac{\partial y}{\partial x_j} s_{\bar{x}_j}\right) \left(\frac{\partial y}{\partial x_k} s_{\bar{x}_k}\right)} \quad (19)$$

where s is the 95% confidence interval (CI), y is the dependent variable, x is the independent variable, n is the number of independent variable, and $r_{x_j x_k}$ is the correlation coefficient between x_j and x_k .

We used a Monte Carlo approach to calculate CI for the L estimates based on allometry and litterfall. For each analysis, we generated 1000 realizations of the estimated value by randomly sampling from normal distributions of the individual variables in the component equation (Harmon et al., 2007). The 95% CI for allometry L included the uncertainty in the 2008 diameter projections and the allometric regression error. For litterfall L , error propagation included the uncertainty in the SLA determination and the spatial variance among the 25 traps.

We present all data as the mean ± 95% CI. If the 95% CIs of the calculated means did not overlap with each other, then they were considered to be significantly different at $\alpha = 0.05$. All statistical analyses were performed using JMP (SAS Institute Inc. v7.0, 2007, Cary, NC, USA) or Splus (TIBCO Spotfire S+ 8.1, Palo Alto, California).

4. Results

4.1. Leaf inclination angle distribution function and leaf projection function

Our measurements of θ_L showed an overall erectophile leaf inclination angle distribution function (Fig. 2a). The mean angle was 62° and it did not vary much with height (Table 2). Based on the measurements, a Beta-distribution function was fitted and the $f(\theta_L)$ was developed (Section 2.1). Finally, we characterized $G(\theta)$ using $f(\theta_L)$ (Eq. (3)). The $G(\theta)$ was close to that of the spherical orientation (black-filled circle in Fig. 2b).

4.2. Gap fraction

Multi-angle P_o values were measured using LAI-2000, TRAC, and DHP and modeled with Nilson (1999) and Kobayashi and Iwabuchi (2008) (Fig. 3a). To improve readability, we did not draw the 95% CI but we interpret the results based on these calculations. The DCP only provided $P_o(0)$, which was not significantly different from LAI-2000 and two gap-fraction models within zero to 13° θ_v . Overall, the estimates of $P_o(\theta_v)$ from LAI-2000, Nilson (1999) and Kobayashi and Iwabuchi (2008) were not significantly different. DHP showed significantly higher P_o values among methods between 40 and 70° θ . TRAC showed significantly lower P_o estimates than LAI-2000, DHP, and Kobayashi and Iwabuchi (2008) between 35 and 65° θ . The P_o estimated from gap size distribution function (Chen and Cihlar, 1995; Leblanc, 2002) agreed well with the ratio of P_o measured below the canopy to P_o measured at the top of tower (linear regression: $y = 0.99x$, $r^2 = 0.84$, $p < 0.001$) (Fig. 3b).

4.3. Element clumping index

We quantified Ω_E using several instruments, models and a theoretical equation (Table 3) and we found considerable difference among them. The Ω_E values were significantly different depending on calculation methods (CLX and CC) for DHP. From Eq. (10), Ω_E can be directly calculated if independent measurements of L_t and L_e exist. L_t from the sum of litterfall L (0.82) and W (0.32, see Section 4.4) was 1.14. Spatially representative L_e at ecosystem scale measured from LAI-2000 was 0.56 (Section 4.5). Thus, Ω_E estimated from L_e/L_t was 0.49 ± 0.02 , which was significantly different from all other methods that reported 95% CI. We determined 0.49 ± 0.02 to be the spatially representative Ω_E . The indirect methods based L_e/L_t can be quantified by combining DCP (for

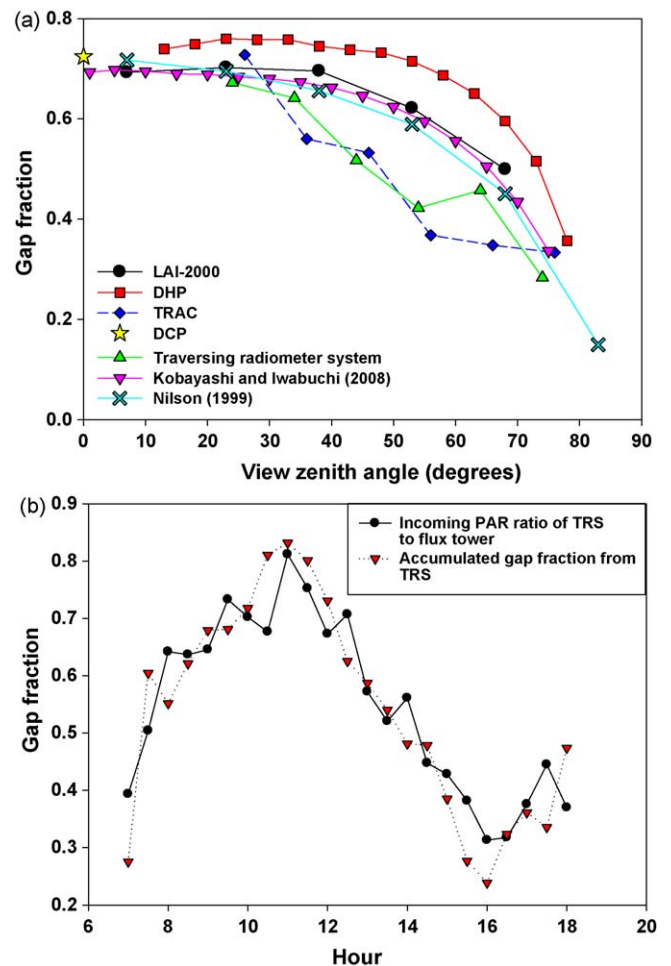


Fig. 3. (a) Gap fraction (P_o) comparison among LAI-2000, DHP, TRAC and DCP sensors with two P_o models using Nilson, 1999 and Kobayashi and Iwabuchi, 2008. To improve readability, 95% CI was not drawn. (b) Comparison between P_o from direct measurement (the ratio of incoming photosynthetically active radiation (PAR) below canopies measured from a traversing radiometer system (TRS) to incoming PAR above canopies measured from top of flux tower) and P_o calculated from accumulated P_o function (Chen and Cihlar, 1995) using the TRS incoming PAR data (sub-box in Fig. 4a) on July 25, 2008. The linear regression between two variables gave $y = 0.99x$ (y : measured, x : calculated, linear regression was forced to pass the origin) with $r^2 = 0.84$.

Table 3Element clumping index (Ω_E) calculated from eight methods. Estimates were reported with mean \pm 95% confidence interval.

	TRAC	DHP	DCP ^a	TRS	Nilson (1999)	Kobayashi and Iwabuchi (2008)	L_e/L_t ^b	DCP-LAI2000 ^c
Ω_E	0.69 \pm 0.07 (CLX) 0.78 \pm 0.09 (CC)	0.57 \pm 0.01 (CLX) 0.79 \pm 0.01 (CC)	0.69 \pm 0.05	0.61 (CLX) 0.72 (CC)	0.54	0.54	0.49 \pm 0.02	0.49 \pm 0.10

^a DCP provides Ω_E at zenith, $\Omega_E(0)$.^b L_e was measured from LAI-2000 and L_t was quantified using litterfall L and DCP based W .^c DCP-LAI2000 uses L_e/L_t relation by using indirect methods; L_e measured from LAI-2000 and L_t measured from DCP. CC indicates Chen and Cihlar (1995) method. CLX is the combination of LX (Lang and Xiang, 1986) and CC methods (Leblanc et al., 2005). DHP is digital hemispheric photography, DCP is digital cover photography, and TRS is traversing radiometer system.

L_t) and LAI-2000 (for L_e) (DCP-LAI2000 in Table 2), and its estimate was 0.49 ± 0.10 .

The angular dependence of Ω_E was tested using TRS, TRAC measurements and three theoretical approaches (Fig. 4). Based on the TRS data, Ω_E decreased with increasing θ (linear regression, $r^2 = 0.15$, $p < 0.01$) (Fig. 4a). On the range between 40 and 70° (θ), Ω_E in the morning were significantly lower than those in the afternoon for CLX whereas there was no significant difference in CC

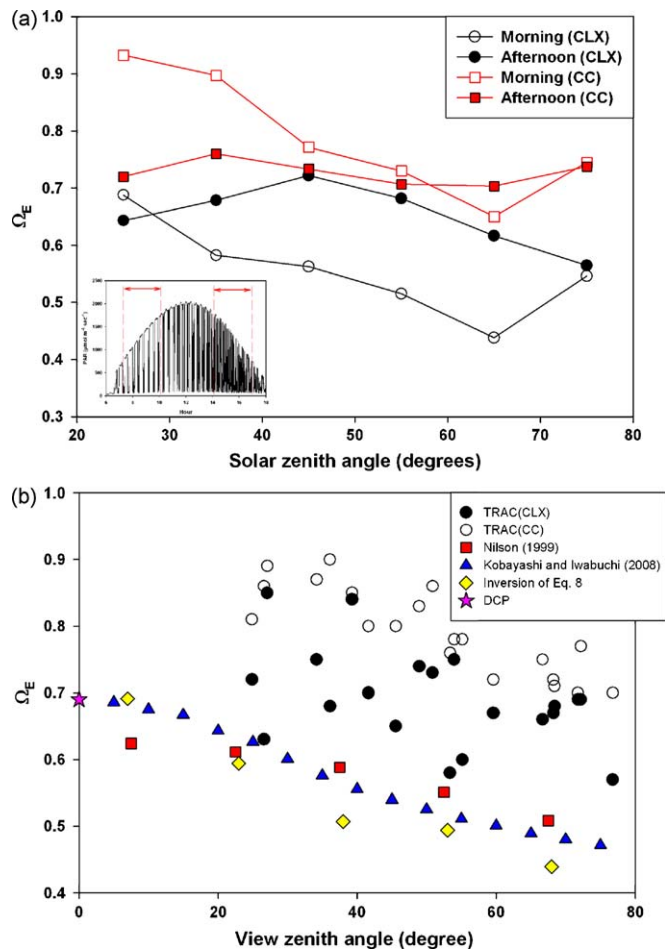


Fig. 4. (a) Element clumping index (Ω_E) with solar zenith angle measured from a traversing radiometer system (DOY 207, 209 and 211 in 2008). All data were grouped into 10 degree intervals of solar zenith angles, and each point represents their mean over three days of measurements. CLX indicates Ω_E from the corrected Lang and Xiang (1986) method (Leblanc et al., 2005). CC indicates Ω_E from Chen and Cihlar (1995) method. The sub-box plot (Fig. 4a) indicates raw incoming photosynthetically active radiation (PAR) data measured from the traversing radiometer system on DOY 209. Within the sub-box plot, red dashed lines indicate 40 and 70° θ . (b) Element clumping index (Ω_E) with view zenith angle, measured from a TRAC sensor, Nilson, 1999, Kobayashi and Iwabuchi, 2008, inversion calculation from Eq. (8), and DCP. (For interpretation of the references to colour in this figure legend, the reader is referred to the web version of the article.)

method. In the morning, big gaps were pronounced whereas incoming PAR fluctuated more in the afternoon (subplot in Fig. 4a). TRAC showed that Ω_E decreased with θ for both CLX and CC methods (linear regression, $r^2 = 0.21$, $p < 0.05$ for CLX, $r^2 = 0.72$, $p < 0.01$ for CC) (Fig. 4b). Nilson (1999), Kobayashi and Iwabuchi (2008) and inversion of Eq. (8) showed that Ω_E decreased with θ (linear regression, $r^2 = 0.89$, $p < 0.001$ for Nilson (1999), $r^2 = 0.98$, $p < 0.0001$ for Kobayashi and Iwabuchi (2008), $r^2 = 0.94$, $p < 0.01$ for inversion of Eq. (8)). DHP-derived $\Omega_E(\theta_v)$ was not used in testing the angular dependence of Ω_E because in 30% of the photographs no leaves were present from 0 to 60° of θ_v due to canopy openness, resulting in undefined Ω_E .

4.4. Woody area index

We quantified W using DCP and Nilson (1999). The W quantified by DCP was 0.32 ± 0.08 . The estimation of Nilson (1999) was 0.24 and 0.05 for B and T , respectively, resulting in W equal to 0.29, which was not significantly different from the DCP estimate ($p > 0.05$). We chose the DCP-based estimate of W because of the associated uncertainty.

4.5. Leaf area index

The comparison of L_e among six methods is presented in Fig. 5a. The L_e derived from DHP was significantly lower than that from LAI-2000. TRAC showed the largest uncertainty of L_e . DCP provided L_e at zenith direction, thus it is not comparable with the other methods. Indirect estimates of L converted from L_e by considering W and Ω_E are given in Fig. 5b. Among indirect estimates of L that reported uncertainty, only DHP (CLX and CC) was significantly different from litterfall and allometry ($p < 0.05$). We did not calculate LAI-2000 based L because our best estimate of Ω_E used L_e/L_t relation where L_e was derived from LAI-2000, thus this way causes circularity fallacy to calculate L .

4.6. Minimum sample size and plot size

We estimated the minimum sample size and plot size to obtain spatially representative P_o and L_e within the 300 m \times 300 m area based on the gridded LAI-2000 measurements (Fig. 1a). The minimum sample size to obtain 5% CV for each ring's P_o was 38, 35, 34, 42 and 63 (Fig. 6a). The CV of 5th ring was significantly higher than the other rings ($p < 0.05$). The CV of L_e decreased with plot size, and 240 m \times 240 m plot size was necessary to obtain 5% CV (Fig. 6b).

5. Discussion

Characterizing L in savannas has remained challenging because most indirect methods assume homogeneous, open canopies. Our results from two direct and five indirect methods and two models demonstrated that a thorough evaluation of P_o between various methods is an essential prerequisite. The pronounced canopy

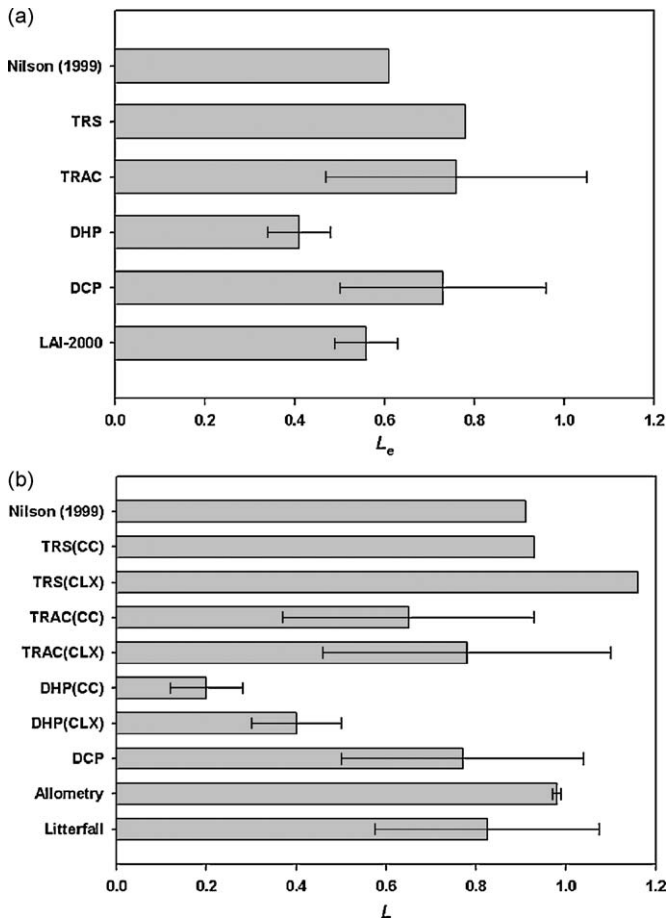


Fig. 5. (a) Effective leaf area index (L_e) comparison among LAI-2000, DCP, DHP, TRAC, TRS and Nilson (1999). DCP provided L_e at zenith direction. (b) Leaf area index (L) comparison among litterfall, allometry, DHP, DCP, TRAC and TRS. CC indicates L calculation using Ω_E derived from Chen and Cihlar (1995). CLX indicates L calculation using Ω_E derived from combination of Chen and Cihlar (1995) and Lang and Xiang (1986) method (Leblanc et al., 2005). DCP is digital cover photography, DHP is digital hemispherical photography, and TRS is traversing radiometer system. Error bars indicate 95% confidence interval.

openness and heterogeneity at our site is characterized by low Ω_E , and large sampling number and extensive plot size that are required to get spatially representative L_e . This result highlights the importance of clumping effect at the ecosystem scale to estimate L adequately in the heterogeneous ecosystem. In the following sections, we answer the questions and provide support in favor or against the hypotheses addressed.

5.1. What are the strengths and weaknesses of multiple methods to assess L in heterogeneous, open canopies?

Among indirect instruments, LAI-2000 was the only one to quantify P_o over a wide range of θ_v reliably (Fig. 3a). This result lends credence to the use of LAI-2000 to acquire spatially representative $P_o(\theta_v)$, and consequently L_e in heterogeneous ecosystem. The conversion of L_e to L_t by LAI-2000 itself may be possible by using LX method (i.e. $\ln(P_o(\theta))$) (Lang and Xiang, 1986). The ratio of L_e calculated from $\ln(P_o(\theta))$ to L_e calculated from $\ln(P_o(\theta))$ was 0.82 ± 0.04 . That is, to some degree, LX method considered clumping effect, yet it was still significantly higher than our best estimate Ω_E (0.49 ± 0.02) ($p < 0.05$). Therefore, independent Ω_E must be quantified and applied to LAI-2000 to convert L_e to L_t . Based on our results, however, no independent method provided reliable Ω_E compared to L_e/L_t (Table 3), thus the

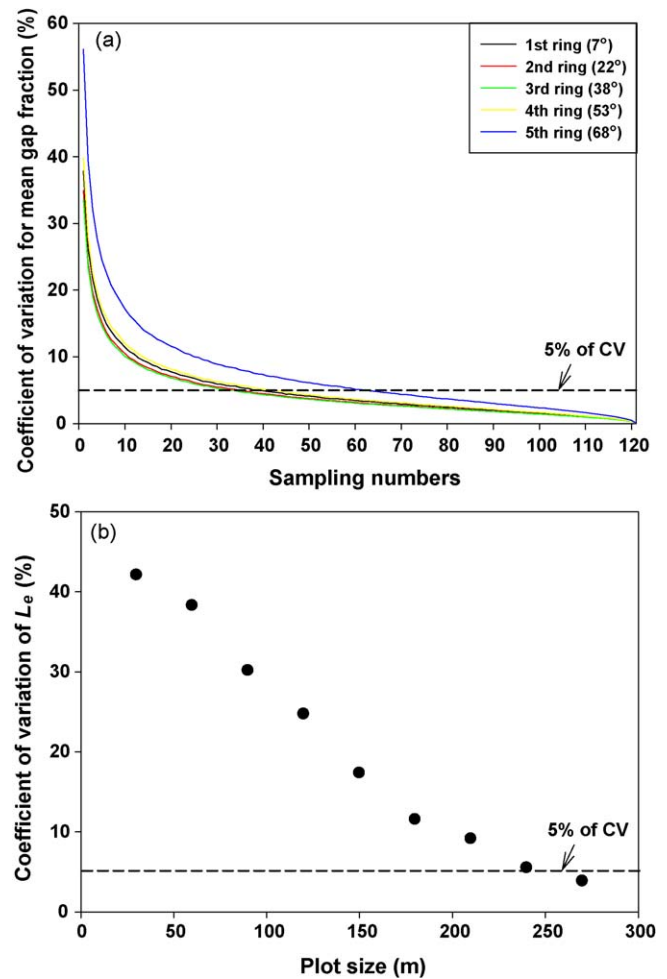


Fig. 6. (a) Coefficient of variation (CV) for mean gap fraction at each view zenith angles in LAI-2000 with sampling numbers. Dashed line indicates 5% of CV. (b) Coefficient of variation of L_e measured from LAI-2000 with window size within the 300 m \times 300 m area (Fig. 1a).

conversion of L_e to L_t in LAI-2000 remains a main challenge in this oak-savanna site.

The DCP provided reliable P_o at zenith. Because of high image resolution and short path length (zenith direction), DCP could identify very small leaves and gaps (Fig. 7a), which gave very accurate $P_o(0)$ (Fig. 3a). Other important strengths of DCP are its ability to quantify Ω_E at zenith and W , which were reliable compared to other methods (see Section 4.3 and Section 4.4). Thus, DCP can quantify L by itself if $f(\theta_l)$ is given. However, it does not have capacity to determine canopy structure over a wide range of θ by only measuring zenith direction. Also, its narrow view angle produced wide error bar (Fig. 5). Comparing DHP that had same sample size (47), 95% CI of DCP was three times greater than that of DHP. Thus, to apply DCP in open canopies, a large sample number is required. Due to the simplicity of DCP measurements that can be made during daylight hours (Macfarlane et al., 2007b), we do not consider the large sample number as a limitation.

The DHP overestimated P_o and underestimated L when compared to the litterfall L . Because of the large number of samples and the large footprint covered by DHP, the 95% CI of L was smallest among all the indirect methods. Specifically, P_o over 40–70° θ_v was significantly higher than other direct and indirect methods (Fig. 3a). A critical limitation of DHP to obtain accurate P_o estimates in this ecosystem is that the short focal distance of the

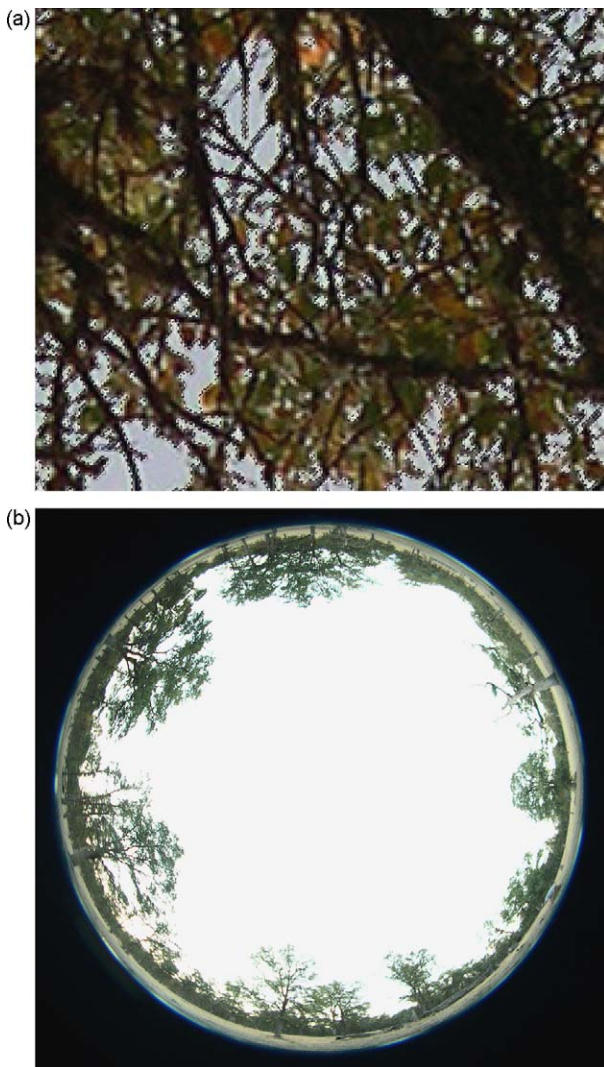


Fig. 7. (a) A subset of an image of Digital Cover Photograph (DCP) taken on Aug 6, 2008. Dashed lines indicate gaps. (b) An image of Digital Hemispheric Photograph (DHP) taken on Aug 6, 2008.

fish eye lens causes image chromatic aberration especially at angles larger than 60° (Frazer et al., 2001). This limitation is critical in ecosystems with open canopies because the most important P_o information is found at those angles (Fig. 7b). Adequate determination of light exposure is also challenging in open canopies. We followed the protocol proposed Zhang et al. (2005) on the determination of light exposure as developed in boreal forests covering a wide range of L_e (0.2–5). Even if this protocol was evaluated at very low L sites, tree distribution at boreal forests is assumed to be different from savannas where trees form clusters and open spaces prevail. In savannas, the canopy openness of the P_o measurement position could be similar with that of the sky reference position, thus attention must be paid in determining diaphragm aperture to avoid over exposure of the image. An important strength of DHP is that this method averages $P_o(\theta_v)$ over a 360° azimuthal direction and a wide range of θ_v , which reduces spatial variability. Finally it is important to consider that the wide spatial average of $P_o(\theta_v)$ using DHP compromises the calculation (underestimation) of L by missing critical information at angles larger than 60° .

The TRAC and TRS had a weakness of its limited field-of-view by using the direct radiation beam. We believe that the gap size

distribution function employed in TRAC and TRS correctly estimated P_o (Fig. 3b) but due to small transect numbers, the P_o did not represent the spatial heterogeneity (Fig. 6a). It is notable that 95% CI of TRAC based L was largest among the seven methods. To overcome the insufficient footprint of TRAC measurement, large sample size is required. However, it will take much time to use TRAC at many transects over a wide range of θ because sun fleck size measurement requires very slow walking speed ($\sim 0.3 \text{ m s}^{-1}$) (Leblanc et al., 2002). RTS had strengths by keeping the sensor speed constant and the sensor leveled, yet due to one sampling transect caused by rail track structure, the quantification of 95% CI on L was not available. Thus, the use of TRAC and TRS may be impractical to obtain spatially representative P_o , L_e and L_t in such a heterogeneous landscape.

The litterfall method provides a direct estimate of L . It is a straightforward approach that is primarily limited by sample size. Relative to the indirect approaches, collecting litterfall takes a great deal of time. Moreover even with a dedicated effort to maintain 25 collectors, we sampled a very small percentage of the total area (0.02%) due to limited resources to analyze litterfall data. We were forced to keep the size of our opening small (on average 0.16 m^2) to restrict access by the cattle that grazed this site. As a consequence in heterogeneous ecosystems like this oak savanna, there is a great deal of spatial variation. Indeed, the differences among collectors accounted for 96% of the observed uncertainty in the estimate of litterfall L . The litterfall plot was one quarter of the LAI-2000 plot size. We compared $P_o(\theta)$ of five rings in LAI-2000 between the litterfall plot area and the other area, and we did not find significant difference ($p > 0.05$). Thus we assumed that litterfall L value can represent the LAI-2000 plot area.

In contrast there was very little statistical uncertainty associated with allometric L because there was no sampling error. All of the trees within the $150 \text{ m} \times 150 \text{ m}$ plot were measured. The confidence intervals were based on propagating the errors associated with projections of the 2008 tree diameters and with the allometric relationship between leaf area and tree diameter reported by Karlik and McKay (2002). However Karlik and McKay (2002) measured blue oak trees in southern California, 280 km from our site. We do not know if or by how much blue oak allometry varies across its range.

5.2. How to estimate spatially representative clumping index in savannas?

The accurate estimation of Ω_E was very critical to convert L_e to L_t in this savanna site. We determined spatially representative Ω_E at the ecosystem scale to be 0.49 ± 0.02 , which is the lowest value reported so far. It indicates that the clumping effect was dominant at the between-crown scale that corresponds with the open nature of savannas. It is notable that the Ω values at boreal coniferous trees are comparable with the value at this site, yet boreal coniferous trees were highly clumped at shoot level and less clumped between crowns level (e.g. $\gamma = 1.6$, $\Omega_E = 0.92$ of black spruce) (Chen et al., 2006). In spite of the importance of Ω_E to quantify L properly, the methodology to quantify spatially representative Ω_E in savannas has been less explored. Only one study used the TRAC instrument to quantify Ω_E in African savannas (Privette et al., 2004).

We used several instruments including TRAC, TRS, DCP and DHP to quantify Ω_E , yet all instruments did not provide spatially representative Ω_E . TRAC ($n = 4$) and TRS ($n = 1$) covered only a small portion of study area whose canopy structure is different from the whole study area as proved by P_o comparison (Fig. 3a). Thus, TRAC and TRS based Ω_E will represent only some local areas and they were significantly different from our best estimate. DCP provided Ω_E only at zenith, thus integral of Ω_E over the hemisphere was not possible. DHP overestimated P_o over 40–

$70^\circ \theta_v$, thus its calculation of Ω_E is unreliable because P_o is a key input parameter to calculate Ω_E when using gap size distribution function (Chen and Cihlar, 1995; Leblanc, 2002). DHP (CLX) based Ω_E was not significantly different from our best estimate ($p > 0.05$), but it is unclear whether it was by correct derivation or by artifact. This analysis highlights that enough sample size and adequate performance of the instruments must be made to get spatially representative Ω_E .

Besides sampling area and performance of instruments, the calculation of Ω_E (i.e. CLX vs CC) needs further investigation to acquire spatially representative Ω_E . The Ω_E calculated from the CLX method was significantly lower than that from the CC method (Table 3). Also, the Ω_E calculated from the CLX method was 0.23 lower than the CC method in 29 boreal forests (Leblanc et al., 2005). Leblanc et al. (2005) advocated the CLX method because it gave a closer L value to the allometry based L estimate. However, in a thinning experiment conducted at an eucalyptus forest, it was reported that $G(\theta)$ changed with thinning whereas Ω did not change in the CLX method, which is hard to explain (Macfarlane et al., 2007b). Here we tested both methods using the TRS data (Fig. 4a). Theoretically, frequent big gaps should lead to lower Ω_E values (Kucharik et al., 1999). Only CLX method presented significantly lower Ω_E in the morning when frequent big gaps prevailed than afternoon (Fig. 4a). Both CC and CLX methods remove large gaps within each segment that can not appear in randomly distributed leaves using the CC method; if the reduced gap size distribution function is still not random after removing the large gaps, then only the CLX method accounts for non-random gaps using the Lang and Xiang (1986) method (Leblanc et al., 2005). Therefore, we support the CLX method which is based on both theoretical and experimental considerations. Because most studies employing TRAC sensor have used the CC method, special attention is required when using Ω_E values from the literature.

In this study, we determined spatially representative Ω_E using L_e/L_t relation. There is a criticism on the derivation of Ω_E using L_e/L_t because the multiple-scattering of light in the canopy at high θ_v can cause erroneous L_e estimate from the LAI-2000 instrument (Chen et al., 1997). However, we believe this is not the case in this savanna site because $P_o(\theta)$ measured from the LAI-2000 was reliable even at the highest θ_v (Fig. 4). We presume that the frequent open space with low L may avoid serious contamination of P_o by the multiple-scattering of light. We confirmed the reliability of Ω_E calculated from L_e/L_t by comparing with the values of Ω_E derived from two P_o models (Table 3). In heterogeneous savannas, L_e/L_t method may be adequate way to acquire spatially representative Ω_E . We suggest combining LAI-2000 (for L_e) and DCP (for L and W) to get spatially representative Ω_E indirectly (DCP-LAI2000 in Table 3). This indirect approach gave 0.49 ± 0.10 , which was not significantly different from L_e/L_t using litterfall L . This approach may be used to validate satellite based regional Ω map that calculated Ω_E based on L_e/L_t relation (Chen et al., 2005).

5.3. Angular dependence of element clumping index

Based on two instruments (TRAC and TRS), two P_o models and an inversion calculation of Eq. (9) (Fig. 3), we found that Ω_E decreased with θ thus we rejected the first hypothesis where the element clumping index may increase with Ω_E .

Several papers reported that Ω_E values change with θ (Andrieu and Sinoquet, 1993; Chen, 1996; Chen et al., 2008; Kucharik et al., 1999; Norman and Welles, 1983) yet the underlying mechanism is still unclear. Previous studies from several boreal needle-leaved forests reported that Ω_E increased with θ (Chen, 1996; Kucharik et al., 1999; Leblanc et al., 2005) and oak and maple trees (Kucharik et al., 1999), which is in contrast to our finding. This trend may be explained by the gap size distribution (Chen, 1996). When

canopies are horizontally dense and vertically prolonged, the path length of a ray through the canopies increases with θ . The longer path length makes large gaps be decomposed into smaller ones, which is close to random gap size distribution (close to 1 of Ω_E). However, this explanation needs to be tested in heterogeneous landscape.

We analyzed the factors influencing the angular dependence of Ω_E (Eq. (16)). The angular trends of Ω_E with θ_v could be caused by factors on leaf, crown and tree distribution pattern levels. We found that the angular dependence of Ω_E was modulated to some degree by ecosystem scale tree distribution patterns, rather than by leaf and crown level. First, in the leaf level, $f(\theta_L)$ could be considered as a potential factor to modulate Ω_E as influencing gap size and P_o through its influence on the G in Eq. (16). Just the erectophile type of leaf angle distribution could cause a decrease in Ω_E along with the view angle θ_v . However, the measured $f(\theta_L)$ was not far from spherical distribution, which indicates angular dependence of Ω_E on $f(\theta_L)$ will be marginal. Second, at the crown level, the crown shape was practically spherical and thus the product $S(\theta_v) \cos \theta_v$ in Eq. (16) was nearly constant with respect to θ_v . Therefore, angular dependence of Ω_E should not much be caused by crown shape. Lastly, the next factor that possibly causes the angular dependence of Ω_E is the tree distribution pattern at ecosystem scale, if the pattern is different when the forest is viewed at different angles. In Eq. (16) the tree distribution pattern effect is characterized by the factor $c(\theta_v)$ which is mainly determined by the relative variance of the number of trees occurring on a subplot whose area is equal to the projection area of the crown envelope (Eq. (14)). A potential dependence of the single-crown gap fraction $P_1(\theta_v)$ (Eq. (15)) on the view angle θ_v is marginal because of spherical crown form and close to spherical leaf orientation. If looking at a sphere at different angles, the path length inside a spherical crown does not depend on the angle. If the trees are regularly spaced, the Ω_E is large. If the trees show a clumped distribution pattern, the Ω_E is smaller. Based on the distribution of tree numbers occurring on a circular subsample of given area (Fig. A1 in Appendix B), the distribution pattern when viewed at near-zenith angles showed a slightly regular pattern up to the angles 8, 22, 37 and 52°. It was close to random at 67° and showed a clumped distribution at 82°. In the vertical view, the pattern seems to be regular because of certain repulsion effect in the pattern. It is notable that trees cannot grow too near to each other. Even if the trees seem to grow in clusters, there seems to be a regular displacement of trees within a cluster. At larger plot sizes corresponding to large view angles (82°), the clustered character of the pattern started to come out, thus giving rise to an increase of the relative variance G_l and a decrease of $c(\theta_v)$ in Eq. (16) and Ω_E along with the view angle θ_v . A closer observation at the site map (Fig. 1a) shows that there are large gaps with no trees surrounded by tree-dense regions. Therefore, we believe that the angular dependence of Ω_E was controlled by ecosystem scale tree distribution patterns to some degree. We suggest that the angular dependence of Ω_E on the ecosystem scale tree distribution might be a unique characteristic in heterogeneous savanna ecosystem.

5.4. Influence of gaps between crowns on total gap fraction

Based on Nilson (1999) model simulation, we found that gaps between crowns at the oak-savanna site dominantly influenced total P_o compared to three other species from sub-boreal region (Fig. A2 in Appendix C). This result is consistent with lower Ω_E at the study site because gaps between crowns dominantly cause the gap size distribution function to deviate from random (Kucharik et al., 1999). Because on average 60% of total gaps were derived from between crowns gaps (Appendix C), indirect instruments

actually measured P_o that is not related with canopies, indicating that the accurate quantification of Ω_E is most important to quantify L in this oak-savanna ecosystem. This simulation analysis highlights the dominance of frequent open spaces in the savanna, thus we support our second hypothesis where the influence of gaps between crowns on total P_o may be dominant in the savanna site.

6. Summary and conclusions

In this study, we quantified tree L using assessments of the probability of beam penetration made with multiple instruments and multiple gap-fraction models in a heterogeneous oak-savanna ecosystem. We demonstrated pronounced heterogeneity at the study site; this was supported by low Ω_E (0.49), large proportion of between-crown gaps (60%), and large minimum sample (63) and plot size (5.8 ha) to obtain spatially representative values of L_e at ecosystem scale. The application of indirect methods in heterogeneous ecosystems such as savannas has been less explored. To acquire spatially representative L and its associated canopy structure variables, we suggest following procedure:

- (1) Characterize $f(\theta_L)$ to quantify G-function.
- (2) Use DCP to estimate $P_o(0)$, $\Omega_E(0)$, L_t , and W to quantify L .
- (3) Use LAI-200 to quantify $P_o(\theta_V)$ and L_e .
- (4) Estimate Ω_E at ecosystem scale using L_e/L_t relation.
- (5) Characterize $\Omega_E(\theta_V)$ using inverse calculation of Eq. (8).

One digital camera that is able to resolve individual leaves as a function of leaf size and distance from tower to the trees-of-interest can be used to quantify $f(\theta_L)$ (our horizontal view digital camera method) and L (DCP method) with confidence in savannas. In-detail canopy structure information may be extracted by combining DCP and LAI-2000. This approach needs to be evaluated at other ecosystems. The use of TRAC and DHP in heterogeneous savannas calls special attention because of the limited footprint covered by the sensor (TRAC) and chromatic aberration at high θ_V with a difficulty to determine light exposure (DHP). To apply TRAC and DHP adequately, their $P_o(\theta_V)$ must be evaluated first with the LAI-2000 or other gap-fraction models. Our results highlight the importance of ecosystem-scale clumping effects for the adequate quantification of tree L in savannas. Furthermore, we showed that the modeling-measurement integration approach was essential to understand canopy structure and light penetration in this oak-savanna ecosystem.

Acknowledgements

We thank Dr. John Norman for constructive comments on leaf inclination angle and clumping index, Dr. Jing Chen and Jan Pisek for the TRAC instrument, Sylvain Leblanc for constructive comments on clumping index in TRAC and DHP, Dr. Craig Macfarlane for helpful comments on digital cover photography, Dr. Qi Chen for providing LiDAR data, Dr. John Battles for analyzing litterfall L data, and Jaclyn Hatala for proofreading this manuscript. Dr. Mait Lang at Tartu Observatory kindly provided his program on tree distribution calculation. We also thank Russell Tonzi for access and use of his ranch for scientific research. Youngryel Ryu was supported by NASA Headquarters under the NASA Earth and Space Science Fellowship Program (NNX08AU25H) and the Berkeley Water Center/Microsoft eScience project. Tiit Nilson was supported by Estonian Science Foundation grant no 6815. This research was conducted at the site that is a member of the AmeriFlux and Fluxnet networks and supported in part by the Office of Science (BER), the U.S. Department of Energy (DE-FG02-03ER63638).

Appendix A

A.1. Nomenclature

B	branch area index
CC	clumping index calculated by Chen and Cihlar (1995)
CLX	clumping index that combines CC and CLX method suggested by Leblanc et al. (2005)
DHP	Digital hemispheric photography
DCP	Digital cover photography (non-fisheye lens)
$f(\theta_L)$	leaf inclination angle distribution function
G	projection coefficient of unit foliage area on a plane perpendicular to the view direction
K	contact number
L_e	effective leaf area index
L_t	total plant area index that includes woody components
L	leaf area index
LX	clumping index calculated by Lang and Xiang (1986)
P_o	gap fraction
RTS	Radiometer traversing system
T	trunk area index
TRAC	Tracing radiation and canopy architecture
W	woody area index
θ	solar zenith angle
θ_V	view zenith angle
θ_L	leaf inclination angle—the angle between leaf normal and zenith
Ω	clumping index
Ω_E	element clumping index

A.2. Distribution of tree numbers occurring on a circular subsample of given area

The distribution of tree numbers occurring on a circular subsample of given area was made using individual tree position within 200-m by 200-m LiDAR data. The mean canopy shape was applied to all individual trees to keep simplicity. Based on the program developed by Dr. Lang (personal communication with Dr. Lang), a circular subsample was randomly dropped on the 200-m by 200-m plot 10,000 times. At each time, the number of trees occurring on this subsample was calculated. The probabilities of occurring 0, 1, 2, 3, ... trees within the subsample was estimated and consequently, mean number, variance and relative variance (Fisher's dispersion index, GI in Eq. (13)) of the distribution was calculated. This process was repeated for subsample areas corresponding to the projection of mean tree crown on the horizontal surface at the θ_V of 8, 22, 37, 52, 67, and 82° (Fig. A1). Tree distribution is characterized as regular ($GI < 1$), random ($GI = 1$) and clumped ($GI > 1$). The result shows that GI were 0.83, 0.82, 0.83, 0.9, 1 and 1.6 for the θ_V of 8, 22, 37, 52, 67, and 82°, respectively.

A.3. Influence of gaps between crowns on total gap fraction

Based on Nilson (1999) model simulation, we quantified gaps between crowns and total gaps. We compared the ratio of gaps between crowns to total gaps at the oak-savanna study site with three other species from sub-boreal region (Fig. A2). Up to 68°, the proportion of between gaps to total gaps exceeded 50% at the oak-study site, which is higher than the other sites. The averaged ratio

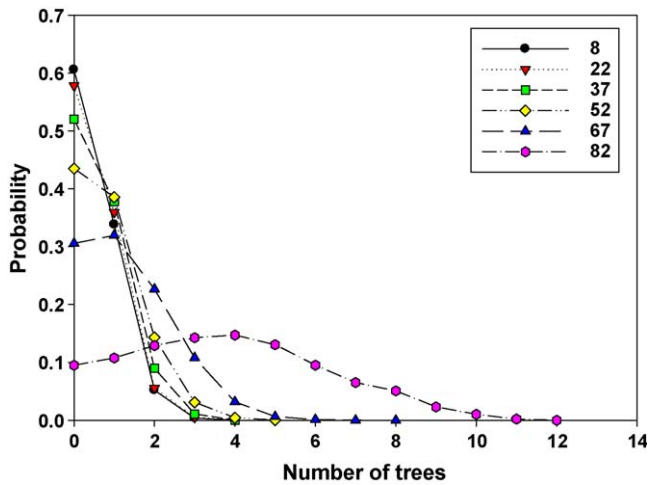


Fig. A1. The probabilities of the number of trees counted in the subsample areas corresponding to the projection of mean tree crown on the horizontal surface at the view zenith angles of 8, 22, 37, 52, 67, and 82.

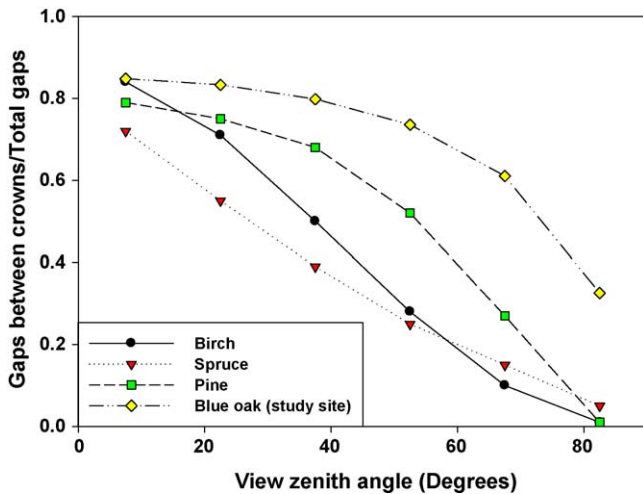


Fig. A2. The ratio of gaps between crowns to total gaps among four tree species simulated by Nilson (1999) model. Canopy covers were 0.8, 0.9, 0.74 and 0.47 for birch, spruce, pine and blue oak, respectively. Data source of birch, spruce and pine is Nilson (1999).

of between crown gaps to total gaps over the hemisphere (i.e. $\sin(\theta)$ weighted) was 60%.

References

- Andrieu, B., Sinoquet, H., 1993. Evaluation of structure description requirements for predicting gap fraction of vegetation canopies. *Agricultural and Forest Meteorology* 65 (3–4), 207–227.
- Aston, A.R., 1979. Rainfall interception by eight small trees. *Journal of Hydrology* 42 (3–4), 383–396.
- Baldocchi, D.D., Fuentes, J.D., Bowling, D.R., Turnipseed, A.A., Monson, R.K., 1999. Scaling isoprene fluxes from leaves to canopies: test cases over a boreal aspen and a mixed species temperate forest. *Journal of Applied Meteorology* 38 (7), 885–898.
- Baldocchi, D.D., Wilson, K.B., Gu, L.H., 2002. How the environment, canopy structure and canopy physiological functioning influence carbon, water and energy fluxes of a temperate broad-leaved deciduous forest—an assessment with the biophysical model CANOAK. *Tree Physiology* 22 (15–16), 1065–1077.
- Baldocchi, D.D., Xu, L.K., 2007. What limits evaporation from Mediterranean oak woodlands—the supply of moisture in the soil, physiological control by plants or the demand by the atmosphere? *Advances in Water Resources* 30 (10), 2113–2122.
- Baldocchi, D.D., Xu, L.K., Kiang, N., 2004. How plant functional-type, weather, seasonal drought, and soil physical properties alter water and energy fluxes of an oak-grass savanna and an annual grassland. *Agricultural and Forest Meteorology* 123 (1–2), 13–39.

- Black, T.A., Chen, J.M., Lee, X.H., Sagar, R.M., 1991. Characteristics of shortwave and longwave irradiances under a Douglas-fir forest stand. *Canadian Journal of Forest Research—Revue Canadienne De Recherche Forestiere* 21 (7), 1020–1028.
- Bonhomme, R., Chartier, P., 1972. Interpretation and automatic measurement of hemispherical photographs to obtain sunlit foliage area and gap frequency. *Israel Journal of Agricultural Research* 22 (2), 53–61.
- Campbell, G.S., 1990. Derivation of an angle density function for canopies with ellipsoidal leaf angle distributions. *Agricultural and Forest Meteorology* 49 (3), 173–176.
- Chen, J.M., 1996. Optically-based methods for measuring seasonal variation of leaf area index in boreal conifer stands. *Agricultural and Forest Meteorology* 80 (2–4), 135–163.
- Chen, J.M., Cihlar, J., 1995. Plant canopy gap-size analysis theory for improving optical measurements of leaf-area index. *Applied Optics* 34 (27), 6211–6222.
- Chen, J.M., Govind, A., Sonnentag, O., Zhang, Y.Q., Barr, A., Amiro, B., 2006. Leaf area index measurements at Fluxnet-Canada forest sites. *Agricultural and Forest Meteorology* 140 (1–4), 257–268.
- Chen, J.M., Menges, C.H., Leblanc, S.G., 2005. Global mapping of foliage clumping index using multi-angular satellite data. *Remote Sensing of Environment* 97 (4), 447–457.
- Chen, J.M., Rich, P.M., Gower, S.T., Norman, J.M., Plummer, S., 1997. Leaf area index of boreal forests: theory, techniques, and measurements. *Journal of Geophysical Research—Atmospheres* 102 (D24), 29429–29443.
- Chen, Q., Baldocchi, D., Gong, P., Dawson, T., 2008. Modeling radiation and photosynthesis of a heterogeneous savanna woodland landscape with a hierarchy of model complexities. *Agricultural and Forest Meteorology* 148 (6–7), 1005–1020.
- Chen, Q., Gong, P., Baldocchi, D., Tian, Y.Q., 2007a. Estimating basal area and stem volume for individual trees from lidar data. *Photogrammetric Engineering and Remote Sensing* 73 (12), 1355–1365.
- Chen, Q., Gong, P., Baldocchi, D., Xie, G., 2007b. Filtering airborne laser scanning data with morphological methods. *Photogrammetric Engineering and Remote Sensing* 73 (2), 175–185.
- de Wit, C.T., 1965. Photosynthesis of Leaf Canopies. *Agricultural Research Report no. 663*, Wageningen.
- dePury, D.G.G., Farquhar, G.D., 1997. Simple scaling of photosynthesis from leaves to canopies without the errors of big-leaf models. *Plant Cell and Environment* 20 (5), 537–557.
- Eagleson, P.S., Segarra, R.I., 1985. Water-limited equilibrium of savanna vegetation systems. *Water Resources Research* 21 (10), 1483–1493.
- Falster, D.S., Westoby, M., 2003. Leaf size and angle vary widely across species: what consequences for light interception? *New Phytologist* 158 (3), 509–525.
- Fassnacht, K.S., Gower, S.T., Norman, J.M., McMurtric, R.E., 1994. A comparison of optical and direct methods for estimating foliage surface area index in forests. *Agricultural and Forest Meteorology* 71 (1–2), 183–207.
- Fisher, R.A., 1954. *Statistical Methods for Research Workers*, Hafner, New York, 356 pp.
- Frazer, G.W., Fournier, R.A., Trofymow, J.A., Hall, R.J., 2001. A comparison of digital and film fisheye photography for analysis of forest canopy structure and gap light transmission. *Agricultural and Forest Meteorology* 109 (4), 249–263.
- Goel, N.S., Strelbe, D.E., 1984. Simple Beta distribution representation of leaf orientation in vegetation canopies. *Agronomy Journal* 76 (5), 800–802.
- Gower, S.T., Norman, J.M., 1991. Rapid estimation of leaf area index in conifer and broad-leaf plantations. *Ecology* 72 (5), 1896–1900.
- Hall, R.J., Davidson, D.P., Peddle, D.R., 2003. Ground and remote estimation of leaf area index in Rocky Mountain forest stands, Kananaskis, Alberta. *Canadian Journal of Remote Sensing* 29 (3), 411–427.
- Harmon, M.E., Phillips, D.L., Battles, J.J., Rassweiler, A., Hall Jr., R.O., Lauenroth, W.K., 2007. Quantifying uncertainty in net primary production measurements. In: *Principles and Standards for Measuring Net Primary Production in Long-Term Ecological Studies*, Oxford University Press, Oxford and New York.
- Hicks, B.B., Baldocchi, D.D., Meyers, T.P., Hosker, R.P., Matt, D.R., 1987. A preliminary multiple resistance routine for deriving dry deposition velocities from measured quantities. *Water Air and Soil Pollution* 36 (3–4), 311–330.
- Hoffmann, W.A., da Silva, E.R., Machado, G.C., Bucci, S.J., Scholz, F.G., Goldstein, G., Meinzer, F.C., 2005. Seasonal leaf dynamics across a tree density gradient in a Brazilian savanna. *Oecologia* 145 (2), 307–316.
- Hosoi, F., Omasa, K., 2007. Factors contributing to accuracy in the estimation of the woody canopy leaf area density profile using 3D portable lidar imaging. *Journal of Experimental Botany* 58 (12), 3463–3473.
- Hutchinson, B.A., Matt, D.R., McMillen, R.T., Gross, L.J., Tajchman, S.J., Norman, J.M., 1986. The architecture of a deciduous forest canopy in eastern Tennessee, USA. *Journal of Ecology* 74 (3), 635–646.
- Idso, S.B., de Wit, C.T., 1970. Light relations in plant canopies. *Applied Optics* 9 (1), 177–184.
- Joffre, R., Rambal, S., Damesin, C., 2007. Functional attributes in Mediterranean-type ecosystems. In: Pugnnaire, F., Valladares, F. (Eds.), *Functional Plant Ecology*, Second Edition. Books in Soils, Plants, and the Environment, CRC Press, Boca Raton, pp. 285–312.
- Jonckheere, I., Muys, B., Coppin, P., 2005. Allometry and evaluation of in situ optical LAI determination in Scots pine: a case study in Belgium. *Tree Physiology* 25 (6), 723–732.
- Karlik, J.F., McKay, A.H., 2002. Leaf area index, leaf mass density, and allometric relationships derived from harvest of blue oaks in a California oak savanna. *USDA Forest Service General Technical Report Number PSW-GTR-184*.

- Kelliher, F.M., Leuning, R., Raupach, M.R., Schulze, E.-D., 1995. Maximum conductances for evaporation from global vegetation types. *Agricultural and Forest Meteorology* 73, 1–16.
- Kim, J., Guo, Q., Baldocchi, D.D., Leclerc, M., Xu, L., Schmid, H.P., 2006. Upscaling fluxes from tower to landscape: overlaying flux footprints on high-resolution (IKONOS) images of vegetation cover. *Agricultural and Forest Meteorology* 136 (3–4), 132–146.
- Kobayashi, H., Iwabuchi, H., 2008. A coupled 1-D atmosphere and 3-D canopy radiative transfer model for canopy reflectance, light environment, and photosynthesis simulation in a heterogeneous landscape. *Remote Sensing of Environment* 112 (1), 173–185.
- Kucharik, C., Norman, J.M., Gower, S.T., 1998a. Measurements of leaf orientation, light distribution and sunlit leaf area in a boreal aspen forest. *Agricultural and Forest Meteorology* 91(1–2), 127–148.
- Kucharik, C.J., Norman, J.M., Gower, S.T., 1998b. Measurements of branch area and adjusting leaf area index indirect measurements. *Agricultural and Forest Meteorology* 91(1–2), 69–88.
- Kucharik, C.J., Norman, J.M., Gower, S.T., 1999. Characterization of radiation regimes in nonrandom forest canopies: theory, measurements, and a simplified modeling approach. *Tree Physiology* 19 (11), 695–706.
- Lang, A.R.G., 1973. Leaf orientation of a cotton plant. *Agricultural Meteorology* 11 (1), 37–51.
- Lang, A.R.G., Xiang, Y., 1986. Estimation of leaf area index from transmission of direct sunlight in discontinuous canopies. *Agricultural and Forest Meteorology* 37 (3), 229–243.
- Lang, A.R.G., Xiang, Y.Q., Norman, J.M., 1985. Crop structure and the penetration of direct sunlight. *Agricultural and Forest Meteorology* 35 (1–4), 83–101.
- Law, B.E., Van Tuyl, S., Cescatti, A., Baldocchi, D.D., 2001. Estimation of leaf area index in open-canopy ponderosa pine forests at different successional stages and management regimes in Oregon. *Agricultural and Forest Meteorology* 108 (1), 1–14.
- Leblanc, S.G., 2002. Correction to the plant canopy gap-size analysis theory used by the Tracing Radiation and Architecture of Canopies instrument. *Applied Optics* 41 (36), 7667–7670.
- Leblanc, S.G., 2008. DHP-TRACwin Manual, Canada Centre for Remote Sensing, Québec, Canada.
- Leblanc, S.G., Chen, J.M., Fernandes, R., Deering, D.W., Conley, A., 2005. Methodology comparison for canopy structure parameters extraction from digital hemispherical photography in boreal forests. *Agricultural and Forest Meteorology* 129 (3–4), 187–207.
- Leblanc, S.G., Chen, J.M., Kwong, M., 2002. Tracing Radiation and Architecture of Canopies TRAC MANUAL Version 2.1.3, Ontario, Canada.
- Leuning, R., Kelliher, F.M., Depury, D.G.G., Schulze, E.D., 1995. Leaf nitrogen, photosynthesis, conductance and transpiration—scaling from leaves to canopies. *Plant Cell and Environment* 18 (10), 1183–1200.
- Ma, S., Baldocchi, D.D., Xu, L., Hehn, T., 2007. Inter-annual variability in carbon dioxide exchange of an oak/grass savanna and open grassland in California. *Agricultural and Forest Meteorology* 147 (3–4), 157–171.
- Macfarlane, C., Grigg, A., Evangelista, C., 2007a. Estimating forest leaf area using cover and fullframe fisheye photography: thinking inside the circle. *Agricultural and Forest Meteorology* 146 (1–2), 1–12.
- Macfarlane, C., Hoffman, M., Eamus, D., Kerp, N., Higginson, S., McMurtrie, R., Adams, M., 2007b. Estimation of leaf area index in eucalypt forest using digital photography. *Agricultural and Forest Meteorology* 143 (3–4), 176–188.
- Marshall, J.D., Waring, R.H., 1986. Comparison of methods of estimating leaf-area index in old-growth douglas-fir. *Ecology* 67 (4), 975–979.
- Miller, J.B., 1967. A formula for average foliage density. *Australian Journal of Botany* 15 (1), 141–144.
- Monsi, M., Saeki, T., 1953. Über den Lichtfaktor in den Pflanzengesellschaften und seine Bedeutung für die Stoffproduktion. *Japanese Journal of Botany* 14, 22–52.
- Monsi, M., Saeki, T., 2005. On the factor light in plant communities and its importance for matter production. *Annals of Botany* 95 (3), 549–567.
- Myneni, R.B., Ross, J., Asrar, G., 1989. A review on the theory of photon transport in leaf canopies. *Agricultural and Forest Meteorology* 45 (1–2), 1–153.
- Neumann, H.H., Den Hartog, G., 1989. Leaf area measurements based on hemispherical photographs and leaf-litter collection in a deciduous forest during autumn leaf-fall. *Agricultural and Forest Meteorology* 45 (3–4), 325–345.
- Nilson, T., 1971. Theoretical analysis of frequency of gaps in plant stands. *Agricultural Meteorology* 8 (1), 25–38.
- Nilson, T., 1999. Inversion of gap frequency data in forest stands. *Agricultural and Forest Meteorology* 98–99, 437–448.
- Nilson, T., Kuusk, A., 2004. Improved algorithm for estimating canopy indices from gap fraction data in forest canopies. *Agricultural and Forest Meteorology* 124 (3–4), 157–169.
- Norman, J.M., 1982. Simulation of microclimates. In: Hatfield, J.L., Thomason, I.J. (Eds.), *Biometeorology in Integrated Pest Management*. Academic Press, New York, USA, pp. 65–100.
- Norman, J.M., Jarvis, P.G., 1974. Photosynthesis in sitka spruce (*Picea-sitchensis* (Bong) carr) 3. Measurements of canopy structure and interception of radiation. *Journal of Applied Ecology* 11 (1), 375–398.
- Norman, J.M., Welles, J.M., 1983. Radiative transfer in an array of canopies. *Agronomy Journal* 75 (3), 481–488.
- Pitman, J., 2006. *Probability*. Spinger, New York, USA.
- Privette, J.L., Tian, Y., Roberts, G., Scholes, R.J., Wang, Y., Caylor, K.K., Frost, P., Mukelabai, M., 2004. Vegetation structure characteristics and relationships of Kalahari woodlands and savannas. *Global Change Biology* 10 (3), 281–291.
- Rodríguez-Iturbe, I., D'Odorico, P., Porporato, A., Ridolfi, L., 1999. Tree-grass coexistence in savannas: the role of spatial dynamics and climate fluctuations. *Geophysical Research Letters* 26 (2), 247–250.
- Ross, J., 1981. *The Radiation Regime and Architecture of Plant Stands*. Junk Publishers, The Hague, 391 pp.
- Ryu, Y., Baldocchi, D.D., Ma, S., Hehn, T., 2008. Interannual variability of evapotranspiration and energy exchanges over an annual grassland in California. *Journal of Geophysical Research-Atmospheres*, 113(D09104): doi:10.1029/2007JD009263.
- Ryu, Y., Nilson, T., Kobayashi, H., Sonntag, O., Baldocchi, D.D., 2009. On the correct estimation of effective leaf area index: does it reveal information on clumping effects? To be submitted to *Agricultural and Forest Meteorology*.
- Sankaran, M., Ratnam, J., Hanan, N.P., 2004. Tree-grass coexistence in savannas revisited—insights from an examination of assumptions and mechanisms invoked in existing models. *Ecology Letters* 7 (6), 480–490.
- Scholes, R.J., Frost, P.G.H., Tian, Y.H., 2004. Canopy structure in savannas along a moisture gradient on Kalahari sands. *Global Change Biology* 10 (3), 292–302.
- Schulze, E.D., Kelliher, F.M., Korner, C., Lloyd, J., Leuning, R., 1994. Relationships among maximum stomatal conductance, ecosystem surface conductance, carbon assimilation rate, and plant nitrogen nutrition—a global ecology scaling exercise. *Annual Review of Ecology and Systematics*, 25, 629.
- Sinoquet, H., Pincebourde, S., Adam, B., Donès, N., Phattaralerphong, J., Combes, D., Ploquin, S., Sangsing, K., Kasemsap, P., Thanisawanyangkura, S., Groussier-Bout, G., Casas, J., 2009. 3-D maps of tree canopy geometries at leaf scale. *Ecology* 90 (1), 283–283.
- Smith, J.A., Berry, J.K., 1979. Optical diffraction analysis for estimating foliage angle distribution in grassland canopies. *Australian Journal of Botany* 27 (2), 123–133.
- Smith, J.A., Oliver, R.E., Berry, J.K., 1977. Comparison of 2 photographic techniques for estimating foliage angle distribution. *Australian Journal of Botany* 25 (5), 545–553.
- Taylor, J.R., 1997. *An introduction to error analysis*, 2nd edition. University Science Books, Sausalito, CA.
- van Gardingen, P.R., Jackson, G.E., Hernandez-Daumas, S., Russell, G., Sharp, L., 1999. Leaf area index estimates obtained for clumped canopies using hemispherical photography. *Agricultural and Forest Meteorology* 94 (3–4), 243–257.
- Wang, W.M., Li, Z.L., Su, H.B., 2007. Comparison of leaf angle distribution functions: effects on extinction coefficient and fraction of sunlit foliage. *Agricultural and Forest Meteorology* 143 (1–2), 106–122.
- Warren Wilson, J., 1959. Analysis of the spatial distribution of foliage by two dimensional point quadrats. *New Phytologist* 58 (1), 92–99.
- Warren Wilson, J., 1960. Inclined point quadrats. *New Phytologist* 59 (1), 1–7.
- Warren Wilson, J., 1967. Stand structure and light penetration. 3. Sunlit foliage area. *Journal of Applied Ecology* 4 (1), 159–165.
- Watson, D.J., 1937. The estimation of leaf area in field crops. *Journal of Agricultural Science* 27, 474–483.
- Welles, J.M., Norman, J.M., 1991. Instrument for indirect measurement of canopy architecture. *Agronomy Journal* 83 (5), 818–825.
- Zhang, Y.Q., Chen, J.M., Miller, J.R., 2005. Determining digital hemispherical photograph exposure for leaf area index estimation. *Agricultural and Forest Meteorology* 133 (1–4), 166–181.